DOI: 10.1002/chem.200901809

Thermal- and Light-Induced Spin Crossover in a Guest-Dependent Dinuclear Iron(II) System

Jarrod J. M. Amoore,[a] Suzanne M. Neville,[b] Boujemaa Moubaraki,[b] Simon S. Iremonger,[a] Keith S. Murray,[b] Jean-François Létard,[c] and Cameron J. Kepert*[a]

Abstract: We previously reported the dinuclear material $[Fe^{II}_2(ddpp)_2(NCS)_4]\cdot 4CH_2Cl_2$ ($\mathbf{1}\cdot 4CH_2Cl_2$; ddpp = 2,5-di(2′,2″-dipyridylamino)pyridine) and its partially desolvated analogue ($\mathbf{1}\cdot CH_2Cl_2$), which undergo two- and one-step spin-crossover (SCO) transitions, respectively. Here, we manipulate the type and degree of solvation in this system and find that either a one- or two-step spin transition can be specifically targeted. The chloroform clathrate $\mathbf{1}\cdot 4CHCl_3$ undergoes a relatively abrupt one-step SCO, in which the two equivalent Fe^{II} sites within the dinuclear molecule crossover simultaneously. Partial desolvation of $\mathbf{1}\cdot 4CHCl_3$ to form $\mathbf{1}\cdot 3CHCl_3$ and $\mathbf{1}\cdot CHCl_3$ occurs through single-crystal-to-single-crystal processes (monoclinic $C2/c$ to $P2_1/n$ to $P2_1/n$) in which the two equivalent Fe^{II} sites become inequivalent sites within the dinuclear molecule of each phase. Both $\mathbf{1}\cdot 3CHCl_3$ and $\mathbf{1}\cdot CHCl_3$ undergo one-step spin transitions, with the former having a significantly higher SCO temperature than $\mathbf{1}\cdot 4CHCl_3$ and the latter, and each has a broader SCO transition than $\mathbf{1}\cdot 4CHCl_3$, attributable to the overlap of two SCO steps in each case. Further magnetic manipulation can be carried out on these materials through reversibly resolvating the partially desolvated material with chloroform to produce the original one-step SCO, or with dichloromethane to produce a two-step SCO reminiscent of that seen for $\mathbf{1}\cdot 4CH_2Cl_2$. Furthermore, we investigate the light-induced excited spin state trapping (LIESST) effect on $\mathbf{1}\cdot 4CH_2Cl_2$ and $\mathbf{1}\cdot CH_2Cl_2$ and observe partial LIESST activity for the former and no activity for the latter.

Keywords: clathrates · host–guest systems · iron · magnetic properties · spin crossover

Introduction

The spin-crossover (SCO) phenomenon, which can occur in d^4–d^7 transition metals, is a type of magnetic switching behavior that can be initiated by external perturbations (i.e., temperature, pressure, and light irradiation).[1,2] Importantly, for the memory, sensory, and electronics industries, SCO materials can display bistability (or a memory effect), where two different electronic states can be accessed at the same temperature depending on the history of the sample.[3,4] From fundamental studies on SCO materials it is now known that solid-state interaction between switching centers plays a significant role in enhancing this bistable behavior.[2,5] Furthermore, it is recognized that interaction between SCO centers within the lattice may be enhanced significantly by directly linking the SCO centers, for example in polynuclear materials.[3,6] Within this rapidly growing area the studies of dinuclear complexes are important, first, as they provide the simplest model for probing the degree of cooperativity between metal centers that are bridged covalently[6–13] and, second, as they offer a means to assess the potential synergy between SCO and magnetic coupling.[6,11,14,15]

Of further interest in the investigation of dinuclear SCO materials is their potential to mimic the unique solvent sensitive behavior of porous framework materials, in particular,

[a] Dr. J. J. M. Amoore, Dr. S. S. Iremonger, Prof. C. J. Kepert
School of Chemistry, The University of Sydney
NSW 2006 (Australia)
Fax: (+61) 29351-4597
E-mail: c.kepert@chem.usyd.edu.au

[b] Dr. S. M. Neville, Dr. B. Moubaraki, Prof. K. S. Murray
School of Chemistry, Monash University
Building 23, Clayton, VIC 3800 (Australia)

[c] Dr. J.-F. Létard
Laboratoire des Sciences Moléculaires
ICMCB (CNRS UPR 9048), Université Bordeaux I
33608 Pessac (France)

Supporting information for this article is available on the WWW under http://dx.doi.org/10.1002/chem.200901809.

when structural integrity can be maintained upon solvent removal/exchange.[5–7,16,17] This demonstrated feature of porous SCO materials (SCOFs)[16,17] is advantageous both towards tuning SCO properties through guest manipulation and, furthermore, in allowing the systematic modification of a single structural feature at a time—this is of particular interest for the assessment of isolated magnetic structural features and is often not possible for mononuclear materials. In the recently reported work on $[Fe_2(ddpp)_2(NCS)_4]\cdot 4\,CH_2Cl_2$ (**1**·4 CH_2Cl_2; ddpp = 2,5-di(2′,2″-dipyridylamino)pyridine) we revealed that such solvation-dependent manipulations are possible in dinuclear materials, whereby both the fully solvated **1**·4 CH_2Cl_2 and partially desolvated **1**·CH_2Cl_2 clathrates were successfully isolated and structurally and magnetically characterized.[7] Here, we further investigate this unique dinuclear clathrate system, which provides a readily accessible range of solvated states, by preparing the chloroform solvated analogue $[Fe_2(ddpp)_2(NCS)_4]\cdot 4\,CHCl_3$ (**1**·4 $CHCl_3$) and subsequently manipulating its degree of solvation in a multi-step fashion to obtain the partially desolvated analogues **1**·3 $CHCl_3$ and **1**·$CHCl_3$. Thus, a family of isostructural materials is formed that differ only in the type and degree of solvation, providing a unique opportunity to derive detailed structure–property relationships.

An additional rich attribute of the dinuclear class of materials is the range of possible magneto-structural consequences available within the one material; there are at least three unique, magnetically accessible states potentially provided in each dinuclear unit (i.e., [HS–HS], [HS–LS] and [LS–LS]; HS = high spin, LS = low spin), in addition to further intermediate magnetic states if magnetic coupling is present.[6,7,9–11,15,18] This is an important consideration for molecular switchtronics applications, an area of molecular materials research that is proceeding alongside that of spintronics, for which spin-coupled molecular clusters, including single-molecule magnets (SMMs) and $[n\times n]$ grids are being actively investigated.[19] The use of molecular switches in digital processes and communications (switchtronics) has largely involved the use of organic fluorescent molecules that switch between two states when stimulated by an input signal, the latter for example being chemical and resulting in an optical (emission) output.[20] This kind of signal transduction mechanism executes, at the molecular level, a logic operation that requires only one input signal (i) and one output signal (o), for example, a NOT two-terminal gate (i, o; 01, 10). The other basic binary logic operations AND (two inputs, one output, i_1, i_2, o; 000, 010, 100, 111) and OR (two inputs, one output, i_1, i_2, o; 000, 011, 101, 111), are two-terminal gates, and have also been reproduced in organic fluorescent molecular switches.[21,22] The same logical operations, and more complex ones, occur, of course, in silicon chip transistors (electrical input and output) and it is the rapid growth in miniaturization of electronic devices for communication of data in electronic and optical circuits that is driving molecular-switch research.

In the context of coordination compound spin-crossover switches, the photomagnetism of mononuclear SCO materials (i.e., the light-induced excited spin state trapping effect, LIESST) allows access to the AND logical operation (the two inputs are i_1, light irradiation, and i_2, magnetic field, the output o is the magnetic response; as indicated above, the output is 1 only when both inputs are 1, otherwise it is 0).[4,21] The photomagnetism of dinuclear materials provides access to further logical operations owing to the larger range of potential spin states. In the broader context of switchtronics, di- and polynuclear spin-crossover materials, with the spin transition(s) being influenced by a range of stimuli, increase the scope of molecular switches markedly compared to purely organic systems. Achieving applications of such materials, at workable temperatures, remains the challenge for the future.

In addition to this, a recent report highlighted the ability to specifically target a range of photomagnetic spin states in dinuclear materials purely through wavelength variation, thus providing additional input variation for logical operations.[23] While the photomagnetism of mononuclear materials has been studied extensively, revealing a simple linear relation between thermal and photoinduced magnetic properties[24,25] ($T(\mathrm{LIESST}) = T_0 - 0.3\,T_{1/2}$, where T(LIESST) is the limiting temperature of the light-induced HS information, $T_{1/2}$ is the thermal spin transition temperature and T_0 is an empirical parameter concerning the geometry of the metal ion),[24–28] there are only a handful of dinuclear SCO materials that have been investigated photomagnetically.[21,29] In this context, it is of interest to extend the investigation of SCO in dinuclear materials to discover if they follow the same linear relationship as mononuclear materials or whether new relationships may exist that might allow an increase in the photomagnetic temperatures towards room temperature for information storage applications. Here we investigate the photomagnetic properties of **1**·4 CH_2Cl_2 and its partially desolvated analogue **1**·CH_2Cl_2.

Results

Thermogravimetric analysis (TGA): TGA of **1**·4 CH_2Cl_2 was reported previously and revealed that the four dichloromethane solvent molecules in the asymmetric unit are lost in a series of steps upon heating.[7] The partially and fully desolvated materials, **1**·CH_2Cl_2 and **1**·Ø CH_2Cl_2, can be attained by heating to 120 and 200 °C, respectively. TGA of **1**·4 $CHCl_3$ revealed that the four chloroform solvent molecules are lost at about 45, 55, 78 and 125 °C, to produce **1**·3 $CHCl_3$, **1**·2 $CHCl_3$, **1**·$CHCl_3$, and **1**·Ø $CHCl_3$, respectively (Figure 1); of these, **1**·3 $CHCl_3$ and **1**·$CHCl_3$ have been isolated and characterized structurally and magnetically.

X-ray crystallography: Details of the single-crystal refinements for **1**·4 $CHCl_3$, **1**·3 $CHCl_3$, and **1**·$CHCl_3$ are given in Table 1 and selected bond lengths are given in Table 2. For each structure, standard parameters that quantify the Fe^{II} coordination geometry are summarized in Table 3; these include the average Fe–N bond length, $\langle d_{Fe-N}\rangle$, and the octa-

Table 1. Crystal data and refinement parameters for **1**·4 $CHCl_3$, **1**·3 $CHCl_3$, and **1**·$CHCl_3$.

	1·4 $CHCl_3$		**1**·3 $CHCl_3$		**1**·$CHCl_3$	
	250 K	123 K	250 K	110 K	250 K	110 K
spin state (Fe1-{Fe1/Fe2})	HS–HS	LS–LS	HS–HS	LS–LS	HS–HS	HS–LS
formula	$Fe_2S_4C_{58}H_{42}N_{18}Cl_{12}$	$Fe_2S_4C_{58}H_{42}N_{18}Cl_{12}$	$Fe_2S_4C_{57}H_{41}N_{18}Cl_9$	$Fe_2S_4C_{57}H_{41}N_{18}Cl_9$	$Fe_2S_4C_{55}H_{39}N_{18}Cl_3$	$Fe_2S_4C_{55}H_{39}N_{18}Cl_3$
M_r [g mol^{-1}]	1656.44	1656.44	1537.07	1537.07	1298.33	1298.33
T [K]	250(2)	123(2)	250(2)	110(2)	250(2)	110(2)
crystal system	monoclinic	monoclinic	monoclinic	monoclinic	monoclinic	monoclinic
space group	$C2/c$	$C2/c$	$P2_1/n$	$P2_1/n$	$P2_1/n$	$P2_1/n$
Z	4	4	4	4	4	4
a [Å]	21.263(8)	21.1692(16)	17.566(4)	17.2244(13)	17.540(12)	17.0780(18)
b [Å]	19.467(7)	19.4550(15)	19.463(5)	19.1358(15)	17.751(12)	17.6005(18)
c [Å]	17.777(7)	17.1055(13)	20.467(5)	20.3444(16)	20.502(14)	20.314(2)
β [°]	106.296(6)	106.6460(10)	106.273(4)	107.0330(10)	104.776(12)	105.594(2)
V [Å^3]	7063(4)	6749.6(9)	6717(3)	6411.4(9)	6172(7)	5881.3(11)
ρ_{calcd} [mg m^{-3}]	1.558	1.630	1.520	1.592	1.397	1.466
μ [mm^{-1}]	1.036	1.084	0.967	1.013	0.788	0.826
data/restraints/parameters	7225/0/424	5759/0/424	13729/0/814	15198/0/814	10510/33/744	13880/0/735
$R(F)$ ($I>2\sigma(I)$, all)	0.0618(0.0781)	0.0524(0.0900)	0.0728(0.1238)	0.0663(0.0963)	0.0881(0.1600)	0.0801(0.1325)
$R_w(F^2)$ ($I>2\sigma(I)$, all)	0.1747(0.1962)	0.1260(0.1605)	0.1909(0.2287)	0.1748(0.1958)	0.2286(0.2958)	0.1950(0.2301)
GoF	1.039	1.083	1.060	1.092	1.093	1.088

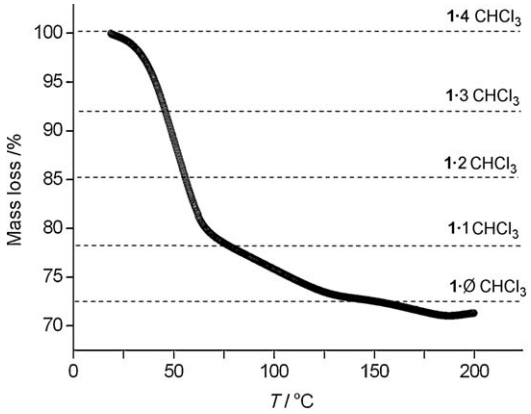

Figure 1. Thermogravimetric data for **1**·4 $CHCl_3$.

Table 2. Selected bond lengths [Å] for **1**·4 $CHCl_3$, **1**·3 $CHCl_3$, and **1**·$CHCl_3$.

	1·4 $CHCl_3$		**1**·3 $CHCl_3$		**1**·$CHCl_3$	
	250 K	123 K	250 K	110 K	250 K	110 K
spin state (Fe1-{Fe1/Fe2})	HS–HS	LS–LS	HS–HS	LS–LS	HS–HS	LS–LS
Fe(1)–N(8/15)[a]	2.108(3)	1.973(5)	2.061(5)	1.952(4)	2.088(7)	1.963(4)
Fe(1)–N(9/16)[a]	2.095(3)	1.975(5)	2.050(5)	1.961(4)	2.095(7)	1.963(4)
Fe(1)–N(1/1)[b]	2.211(3)	2.008(4)	2.136(4)	1.978(3)	2.2116(6)	1.978(4)
Fe(1)–N(3/3)[b]	2.222(3)	2.026(4)	2.152(4)	1.995(3)	2.234(6)	2.006(4)
Fe(1)–N(4/11)[b]	2.200(3)	2.020(4)	2.136(4)	1.988(3)	2.216(5)	2.002(4)
Fe(1)–N(5/12)[b]	2.212(3)	2.021(5)	2.137(5)	1.985(4)	2.200(7)	1.985(4)
Fe(2)–N(-/17)[a]	–	–	2.096(5)	1.974(4)	2.075(7)	2.059(6)
Fe(2)–N(-/18)[a]	–	–	2.087(5)	1.968(4)	2.089(7)	2.074(5)
Fe(2)–N(-/10)[b]	–	–	2.240(5)	2.016(4)	2.227(6)	2.178(4)
Fe(2)–N(-/8)[b]	–	–	2.197(4)	1.991(3)	2.206(6)	2.134(4)
Fe(2)–N(-/5)[b]	–	–	2.219(5)	2.014(4)	2.223(7)	2.169(5)
Fe(2)–N(-/4)[b]	–	–	2.200(4)	2.006(3)	2.239(6)	2.185(4)

[a] N from NCS. [b] N from pyridine.

hedral distortion parameter, Σ (defined as the sum of the deviation of the 12 *cis* N-Fe-N angles around the metal atom from 90°).[30] Intra- and intermolecular π–π-stacking distances are summarized in Table 3 (see also Table S1, S2 and S3 in the Supporting Information for intermolecular hydrogen bonding distances).

Structural analysis of the materials **1**·4 $CHCl_3$, **1**·3 $CHCl_3$, and **1**·$CHCl_3$ revealed dinuclear units comprising the same dinuclear structural motif as **1**·4 CH_2Cl_2, consisting of two iron atoms bridged by two ddpp ligands in a head-to-tail fashion and *cis*-coordinated NCS ligands (Figure 2). The principle structural difference of the dinuclear unit in **1**·4 $CHCl_3$ (monoclinic space group $C2/c$) compared to those seen in the previously reported analogues **1**·4 CH_2Cl_2 and **1**·CH_2Cl_2, is the presence of a local C_2 symmetry resulting in the asymmetric unit containing one half of a dinuclear unit, with the other being generated by twofold rotation (Figure 2a). In contrast, the asymmetric units of **1**·4 CH_2Cl_2 and **1**·CH_2Cl_2 (triclinic space group $P\bar{1}$) each contain one entire dinuclear unit (Figure 2b). This is similarly observed here for the partial solvates **1**·3 $CHCl_3$ and **1**·$CHCl_3$, which each have primitive monoclinic symmetry (space group $P2_1/n$) such that the local C_2 symmetry of the dinuclear unit is broken and an entire dinuclear unit is located in the asymmetric unit (Figure 2b). Thus, **1**·3 $CHCl_3$ and **1**·$CHCl_3$ contain two unique iron centers per dinuclear unit and **1**·4 $CHCl_3$ contains two identical iron centers—an important point in the consideration of their magnetic behaviors.

1·4 $CHCl_3$: The Fe–N bond lengths at 123 and 250 K (Table 2 and 3) are indicative of dinuclear units in the [LS–LS] and [HS–HS] states, respectively.[2]

The dinuclear complexes are held together by a series of intramolecular π–π-stacking interactions (three per dinuclear unit) and adjacent complexes are bridged through in-

Table 3. Comparison of selected inter- and intramolecular parameters for **1**·4 $CHCl_3$, **1**·3 $CHCl_3$, and **1**·$CHCl_3$.

	1·4 $CHCl_3$		**1**·3 $CHCl_3$		**1**·$CHCl_3$	
	250 K	123 K	250 K	110 K	250 K	110 K
spin state (Fe1-{Fe1/Fe2})	HS–HS	LS–LS	HS–HS	LS–LS	HS–HS	LS–HS
T [K]	250(2)	123(2)	250(2)	110(2)	250(2)	110(2)
intramolecular Fe···Fe distance [Å]	7.434(3)	7.233(15)	7.373(2)	7.143(9)	7.371(5)	7.212(11)
$\langle d_{Fe(1)-N}\rangle$ [Å]	2.175(3)	2.004(5)	2.113(4)	1.977(3)	2.174(6)	1.984(4)
$\langle d_{Fe(2)-N}\rangle$ [Å]	–	–	2.173(4)	1.995(3)	2.179(6)	2.113(4)
$\Sigma_{Fe(1)}$ [°][a]	48.46	30.23	34.2	27.7	42.8	25.4
$\Sigma_{Fe(2)}$ [°][a]	–	–	51.3	34.4	47.2	43.6
intramolecular π–π stacking [Å]	3.217(3), 3.411(2)	3.230(2), 3.334(3)	3.352(2), 3.348(7), 3.368(8)	3.246(7), 3.295(6), 3.333(4),	4.096(5), 3.738(4), 3.900(5)	3.937(3), 3.587(3), 3.754(3)
intermolecular π–π stacking [Å]	3.823(3)	3.733(3)	3.644(4)	3.580(10)	3.701(4)	3.632(3)

[a] Σ = sum of the deviation of the 12 *cis* N-Fe-N angles around the metal atom from 90°.

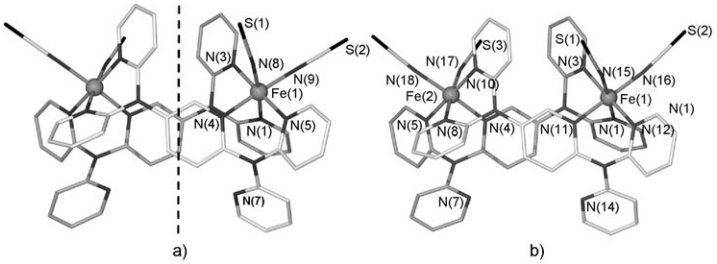

Figure 2. The general dinuclear structure for a) **1**·4 $CHCl_3$, which has crystallographic C_2 symmetry (indicated by the dashed line), and b) **1**·3 $CHCl_3$ and **1**·$CHCl_3$, which each contain an entire dinuclear moiety in the asymmetric unit. The unique Fe, S and N atoms are labelled. Hydrogen and solvent atoms have been omitted for clarity.

termolecular π–π stacking interactions (two per dinuclear unit; Table 3) and (NC)S···H(py) hydrogen-bonding interactions (Table S1 in the Supporting Information). Hydrogen-bonding interactions also exist between the $CHCl_3$ molecules and the dinuclear complexes (Table S1 in the Supporting Information).

***1**·3 $CHCl_3$*: The selective removal of one chloroform solvent molecule from **1**·4 $CHCl_3$ to form **1**·3 $CHCl_3$, results in an effective alteration of the crystallographic symmetry from $C2/c$ to $P2_1/n$ (Figure 3). The Fe–N bond lengths for each inequivalent Fe atom at 110 and 250 K (Table 2 and 3) are slightly shorter than those of **1**·4 $CHCl_3$ and are indicative of dinuclear units in the [LS–LS] and [HS–HS] states, respectively.[2] The octahedral distortion parameters highlight the difference between the iron atoms within each dinuclear unit (Table 3).

Overall, there is minimal change to the structural packing from that of **1**·4 $CHCl_3$, despite a reduction in the unit cell volume, at 250 K, of 346 $Å^3$ (corresponding to 86 $Å^3$ per $CHCl_3$ molecule lost). With the exception of a dinuclear complex–solvent hydrogen-bonding interaction, the intramolecular π–π stacking interactions and network of intermolecular π–π and hydrogen-bonding contacts is retained through this transition, with some subtle changes in contact distances (Table 3 and Table S2 in the Supporting Information).

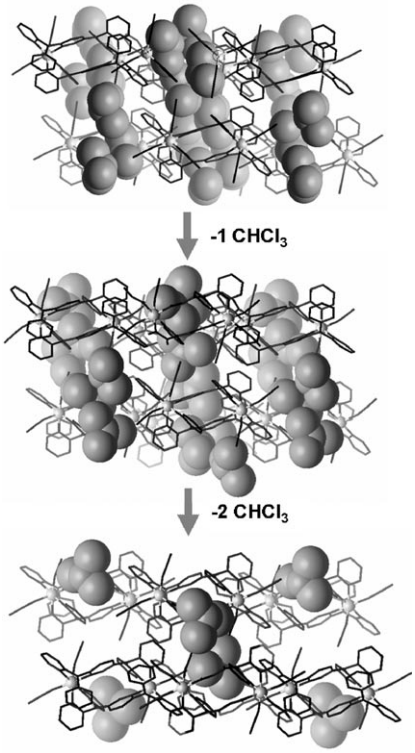

Figure 3. Comparative structural representation of the two-step desolvation process from **1**·4 $CHCl_3$ → **1**·3 $CHCl_3$ → **1**·$CHCl_3$. The location of solvent molecules within each unit cell is shown in space-filling representation.

***1**·$CHCl_3$*: The removal of two additional $CHCl_3$ molecules from **1**·3 $CHCl_3$ to produce **1**·$CHCl_3$ results in a structure that retains the monoclinic $P2_1/n$ space group (Figure 2b and Figure 3). The Fe–N bond lengths at 110 and 250 K (Table 2 and 3) are indicative of dinuclear units in the [LS–HS] and [HS–HS] states, respectively.[2] The octahedral distortion parameters further support a [LS–HS] state in the dinuclear unit at 110 K (Table 3).

Throughout the desolvation process from **1**·4 $CHCl_3$ to **1**·$CHCl_3$ there is a reduction of the unit cell volume, at 250 K, of 891 $Å^3$, corresponding to 74 $Å^3$ per $CHCl_3$ mole-

cule lost. As with **1**·3 $CHCl_3$, the structural packing remains largely unchanged, with the network of intermolecular contacts between the dinuclear complexes being retained (Table 3). There are considerably fewer hydrogen bonds in this material than in **1**·3 $CHCl_3$ and **1**·4 $CHCl_3$ due to the reduced number of solvent molecules present per dinuclear unit (Figure 3 and Table S3 in the Supporting Information).

Thermally induced magnetic susceptibility

1·4 $CHCl_3$: Magnetic susceptibility measurements showed a relatively gradual one-step SCO (Figure 4). The $\chi_M T$ values remained constant at 3.35 $cm^3 K mol^{-1}$ above 210 K, indicative of HS iron(II). With cooling between 210 and 100 K the $\chi_M T$ values decreased to 0.07 $cm^3 K mol^{-1}$, indicative of LS iron(II). Below 100 K the $\chi_M T$ values remained constant at 0.07 $cm^3 K mol^{-1}$. The $T_{1/2}$ value for this material is 148 K.

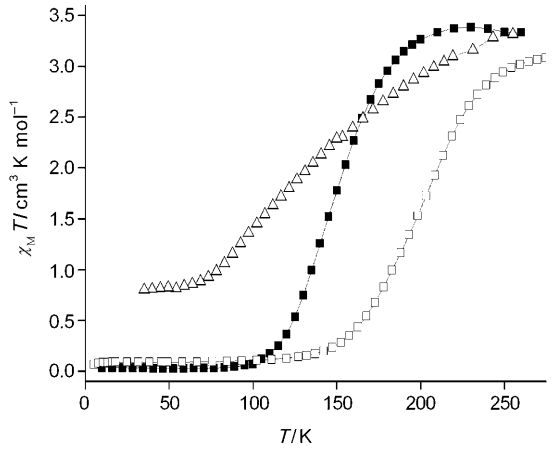

Figure 4. Plot of $\chi_M T$ versus temperature over the range 4–275 K for **1**·4 $CHCl_3$ (■), **1**·3 $CHCl_3$ (□), and **1**·$CHCl_3$ (△).

1·3 $CHCl_3$: Magnetic susceptibility measurements showed a more gradual one-step SCO than **1**·4 $CHCl_3$, with a $T_{1/2}$ value shifted to higher temperatures ($T_{1/2}$ = 200 K, Figure 4). The $\chi_M T$ values remained constant at 3.08 $cm^3 K mol^{-1}$ above 270 K, indicative of HS iron(II). With cooling between 270 and 135 K the $\chi_M T$ values decreased to 0.17 $cm^3 K mol^{-1}$, indicative of LS iron(II). Below 135 K the $\chi_M T$ values remained constant.

1·$CHCl_3$: Magnetic susceptibility measurements showed a gradual incomplete SCO (Figure 4). The $\chi_M T$ values of 3.32 $cm^3 K mol^{-1}$ at 250 K are indicative of HS iron(II). Between 250 and 65 K, the $\chi_M T$ values decreased gradually to reach a minimum of 0.88 $cm^3 K mol^{-1}$, indicative of ca. 75% of the iron(II) sites in the LS state. Below 65 K, the $\chi_M T$ values remained constant at 0.80 $cm^3 K mol^{-1}$.

1·Ø $CHCl_3$: Magnetic susceptibility measurements showed a HS character over the whole temperature range with $\chi_M T$ values remaining constant at 3.20 $cm^3 K mol^{-1}$; this is in accordance with the observation for **1**·Ø CH_2Cl_2.[7]

1·3 $CHCl_3$ resolvated with CH_2Cl_2: Magnetic susceptibility measurements showed a gradual two-step SCO essentially indistinguishable from that reported for **1**·4 CH_2Cl_2 (Figure 5).[7] The $\chi_M T$ values remained constant at 3.20 $cm^3 K mol^{-1}$ above 220 K, indicative of HS iron(II). With cooling between 220 and 135 K the $\chi_M T$ values decreased to 1.75 $cm^3 K mol^{-1}$, indicative of half the iron(II) centers in the LS state. Between 135 K and 50 K, the $\chi_M T$ values decreased further to 0.25 $cm^3 K mol^{-1}$, indicative of all the iron(II) sites in the LS state. Below 50 K the $\chi_M T$ values remained constant. The $T_{1/2}$ values for this material are 168 and 88 K.

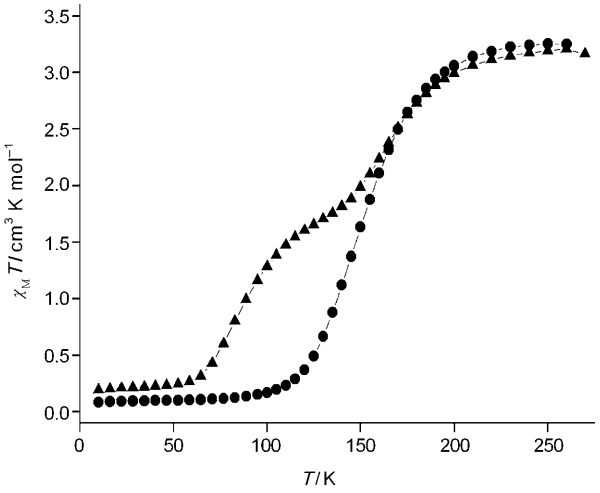

Figure 5. Plot of $\chi_M T$ versus temperature over the range 4–275 K for **1**·CH_2Cl_2 resolvated with $CHCl_3$ (●) and **1**·$CHCl_3$resolvated with CH_2Cl_2 (▲).

1·CH_2Cl_2 resolvated with $CHCl_3$: Magnetic susceptibility measurements showed a gradual one-step SCO (Figure 5). The $\chi_M T$ values remained constant at 3.26 $cm^3 K mol^{-1}$ above 215 K, indicative of HS iron(II). With cooling between 215 and 90 K the $\chi_M T$ values decreased to 0.14 $cm^3 K mol^{-1}$, indicative of LS iron(II). Below 90 K, the $\chi_M T$ values remained constant. The $T_{1/2}$ value for this material is 150 K.

Optical reflectivity: The spectral changes with temperature variation and in the presence of white light for **1**·4 CH_2Cl_2 are shown in Figure 6, where the thermal- and light-induced SCO have been monitored by using the bands at λ = 550 and 830 nm. Over a temperature range of 200–70 K the λ = 550 nm band increased in intensity and the λ = 830 nm band decreased. Over the range 70–10 K these same bands showed the opposite effect, suggesting partial LIESST activity of the HS sites at these temperatures. This is further highlighted when the temperature dependence of the relative absorbance at 550 nm is followed (Figure 6, inset). The band shows a gradual decrease over the range 200–70 K, consis-

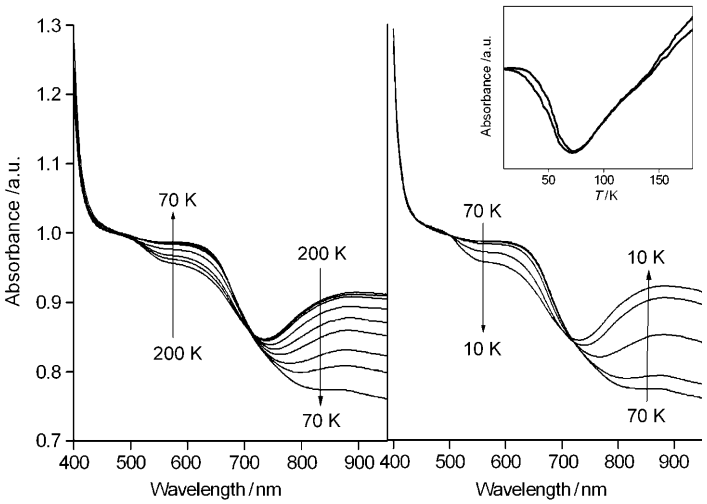

Figure 6. Diffuse absorption spectra for **1**·4 CH_2Cl_2 for the thermal SCO (left) and the LIESST effect (right) over a temperature range of 10–200 K at $\lambda = 400$–950 nm and at a single wavelength ($\lambda = 550$ nm, inset).

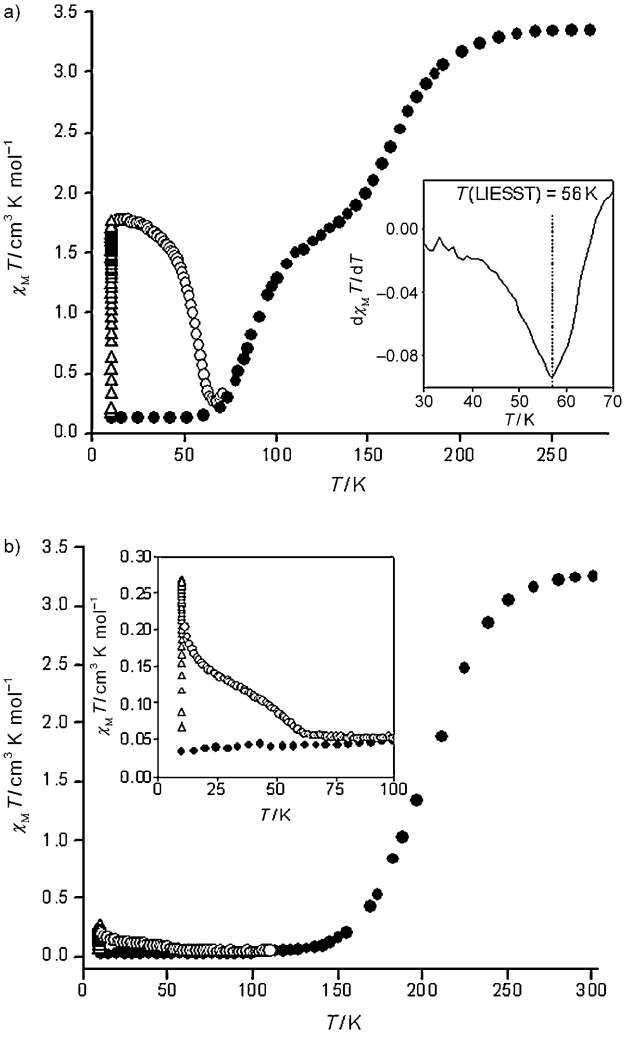

Figure 7. Plot of $\chi_M T$ versus temperature over the range 10–275 K for the thermal and photomagnetic effect of a) **1**·4 CH_2Cl_2 and b) **1**·CH_2Cl_2). Inset of a) Plot of $d\chi_M T/dT$ versus temperature indicating a T(LIESST) value of 56 K at the minima and b) expanded view over the range 10–100 K of the small amount of LIESST effect (△ = irradiate, ○ = T(LIESST), and ● = thermal spin transition).

tent with the observation of the magnetical properties, providing a subtle indication of two-step SCO behavior, followed by an increase to 10 K of approximately 75 % of the intensity measured at 200 K. No LITH (light-induced thermal hysteresis)[31] was observed with repeated heating and cooling cycles. The slight difference in the heating and cooling curves over all temperatures is attributed to a thermal effect.

Light-induced magnetic susceptibility: The magnetic response of **1**·4 CH_2Cl_2 to light irradiation was followed directly through magnetic susceptibility measurements (Figure 7a). A thin layer of the sample irradiated at 10 K showed an increase in $\chi_M T$ to a value of 1.56 cm^3 K mol^{-1}. With heating in the absence of irradiation, the magnetic signal increased slightly owing to zero-field splitting of the HS iron(II) centers; this value corresponds to about 43 % trapping of a metastable HS species at low temperatures—an amount reduced compared to the optical reflectivity. With further heating the metastable HS sites relaxed to attain a minimum $\chi_M T$ value of 0.45 cm^3 K mol^{-1} at 65 K. The T(LIESST) value, calculated from the minimum in the $d\chi_M T/dT$ versus temperature curve, is 56 K (Figure 7a, inset). With a further heating and cooling cycle (10–275 K) the $\chi_M T$ values followed the path of that observed for the original thermal variation. The LIESST effect was then followed by the same method for the partially desolvated sample **1**·CH_2Cl_2, and showed a minimal increase in the $\chi_M T$ values with irradiation at 10 K (Figure 7b).

In further measurements, the time-dependent relaxation kinetics of the light-induced HS fraction were followed for **1**·4 CH_2Cl_2 at 10, 50, 53, 55, 58, and 60 K (Figure 8). The relaxation curves at 50, 53, 55, 58, and 60 K were analysed by using a stretched exponential treatment such that the apparent activation energy, E_a, is 403 cm^{-1} and the pre-exponential factor of the activated region, k_∞, is 1.9×10^3 s^{-1}, with a Gaussian distribution σ of 35 cm^{-1}. These parameters are indicative of relatively weak interaction between the Fe^{II} SCO centers in this material.[26]

Discussion

Over this series of dinuclear materials, which includes the previously reported **1**·4 CH_2Cl_2 and its partially desolvated analogue **1**·CH_2Cl_2,[7] and the new complex **1**·4 $CHCl_3$ and its partially desolvated analogues **1**·3 $CHCl_3$ and **1**·$CHCl_3$, it is evident that guest molecules play an integral role in both the structure and SCO behavior of this systems. Owing to the array of such properties observed within this now expanded family, a number of magneto-structural correlations are now apparent, in particular involving the occurrence of

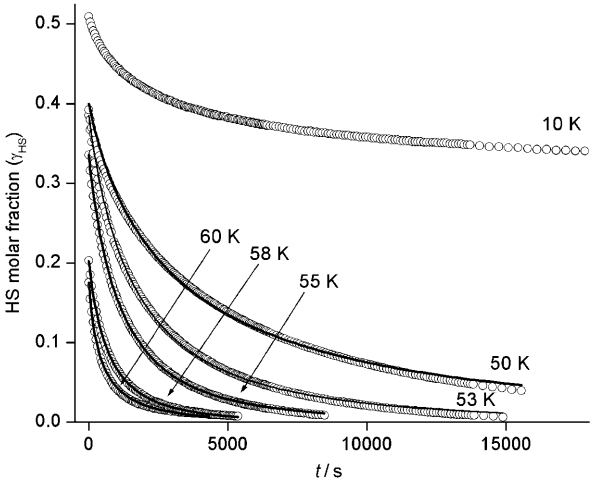

Figure 8. Time-dependent relaxation of the LIESST-induced HS fraction in **1**·4 CH_2Cl_2 at 10, 50, 53, 55, 58, and 60 K.

one- and two-step spin transitions.[9,13] This comparative study has been possible largely due to the remarkably robust nature of this discrete dinuclear material, which is reminiscent of that observed in porous SCO framework materials (SCOFs).[5,16,17]

In assessing the various structural features observed over this series, the most obvious distinction lies in the presence of one or two crystallographically distinct Fe^{II} centers per discrete dinuclear moiety. We observed previously in the parent material **1**·4 CH_2Cl_2, which undergoes a two-step SCO, the presence of two unique Fe^{II} centers per dinuclear unit at all temperatures, which proceed structurally through the process [HS–HS] → [HS–LS] → [LS–LS]. In this material the octahedral distortion parameters of individual Fe^{II} centers are about 45° for HS and about 30° for LS. In contrast, in the chloroform clathrate **1**·4 $CHCl_3$, which undergoes a one-step SCO, the Fe^{II} centers in each dinuclear are equivalent and proceed directly from [HS–HS] → [LS–LS] states (based on $\langle d_{Fe-N} \rangle$ values, Table 3). The octahedral distortion parameters are of the expected magnitude for HS and LS states (48.46 and 30.23°, respectively) and comparable to those of **1**·4 CH_2Cl_2. The observation of similar SCO abruptness for the individual two-step and one-step transitions in **1**·4 CH_2Cl_2 and **1**·4 $CHCl_3$ (Figure 4 and 5), respectively, indicates that intramolecular communication between the inequivalent/equivalent iron centers in each phase is at most negligible, and that it is the crystallographic environment of the dinuclear moieties rather than steric and/or electronic factors within these that principally determines the SCO behavior. This situation contrasts with that seen for example in $[Fe_2(pmat)_2][BF_4]_4$·DMF (pmat = 4-amino-3,5-bis{[(2-pyridylmethyl)amino]methyl}-4*H*-1,2,4-triazole) in which crystallographically equivalent Fe^{II} sites within a dinuclear complex split into HS and LS sites upon cooling through a one-step half SCO transition.[8] Such a difference in behavior reflects the greater intramolecular separation between the iron centers in **1**·*x* guest, resulting in a minimal communicative effect both sterically and electronically; the former is consistent with our previous finding that SCO at each of the two iron sites in **1**·4 CH_2Cl_2 causes negligible change to the coordination geometry of the other.[7]

For the partially desolvated materials **1**·3 $CHCl_3$ and **1**·$CHCl_3$, which show full and incomplete one-step spin transitions, respectively, the magneto-structural correlations are more complex due to the lowering of the symmetry from *C*2/*c* in the parent phase to $P2_1/n$. Despite the emergence of two inequivalent Fe^{II} sites in each case, the SCO transitions remain single step for each; this contrasts with the situation seen in **1**·4 CH_2Cl_2[7] (Figure 4). However, there is a clear broadening of the transition in each case, a feature that we ascribe principally to the overlap of two separate SCO transitions—one from each distinct iron site. For **1**·$CHCl_3$ this broadening is particularly pronounced, suggesting that a degree of crystal inhomogeneity, as associated with partial desolvation, may contribute; the fact that the transition sharpens again upon resolvation indicates that irreversible crystal damage does not add significantly to any heterogeneity.

Notably, the SCO transition temperature for **1**·3 $CHCl_3$ is increased significantly, about 50 K, over that of **1**·4 $CHCl_3$, **1**·$CHCl_3$, and **1**·4 CH_2Cl_2. The presence of an elevated SCO transition can be rationalized when we examine the $\langle d_{Fe-N} \rangle$ and Σ values for the individual Fe^{II} centers. In particular, the values for Fe(1) in the HS state (2.113(4) Å and 34.2°, respectively, at 250 K) are considerably lower than those for other members of this series, reflecting a stabilization of the LS state. Therefore, it seems likely that the broadened one-step SCO is a result of the overlap of the HS-to-LS transition for Fe(1) followed by Fe(2) upon cooling. This situation is similar to that for the previously reported partially-desolvated analogue **1**·CH_2Cl_2, which also shows an elevated one-step SCO with two distinct Fe^{II} centers per dinuclear unit; however, in that case the $\langle d_{Fe-N} \rangle$ and Σ values for each Fe^{II} center were more comparable than those observed here. Interestingly, the elevation of the SCO transition temperature with desolvation seen in these phases contrasts with the situation commonly seen for other desolvated SCO materials, in which destabilization of the LS state occurs.[16,32]

In contrast to the other chloroform clathrates, **1**·$CHCl_3$ undergoes an incomplete SCO transition (ca. 75%). This likely arises with the thermal trapping of residual HS Fe^{II} sites below about 70 K. The influence of the inequivalent Fe^{II} sites on the SCO behavior is clearly seen through analysis of the temperature-dependent structure change, which proceeds in one step from [HS–HS] to [LS–HS] (as evidenced by the $\langle d_{Fe-N} \rangle$ values in Table 3); we note that the structural analysis carried out at 110 K is not at the base of the plateau and magnetically represents 50% SCO at that temperature. The respective octahedral distortion parameters of the Fe^{II} centers at each temperature are of the magnitude expected (Table 3).

All of the complexes studied here display inter- and intramolecular π–π stacking interactions, which provide a robust platform for the retention of crystallinity with solvent re-

moval. Independent of the degree or type of solvent present in the dinuclear moieties, each phase contains three intermolecular π–π stacking interactions, involving those between the central pyridine rings of the two ddpp ligands and between unbound pyridyl rings on each ligand and bound terminal pyridyl rings on the other ligand. On the other hand, due to the varying amounts and type of solvent in each analogue and the associated changes in crystal packing, subtly different intramolecular interactions are present, including those between adjacent dinuclear molecules and with the solvent molecules. This is highlighted in the stepwise reduction of the unit cell volume over the transition **1**·4 $CHCl_3$ → **1**·3 $CHCl_3$ → **1**·$CHCl_3$ of first 346 Å^3 with the loss of four $CHCl_3$ molecules per unit cell and second 545 Å^3 with a further loss of eight $CHCl_3$. This robust nature is further highlighted by following the magnetic consequences of guest exchange in, firstly, **1**·$CHCl_3$ resolvated with CH_2Cl_2 and, secondly, **1**·CH_2Cl_2 resolvated with $CHCl_3$. In the former case a two-step SCO closely similar to that of **1**·4 CH_2Cl_2 is observed, and in the latter case a one-step SCO closely similar to that of **1**·4 $CHCl_3$ is seen. Thus, in this dinuclear system we are able to selectively tune the SCO nature to a one- or two-step character based on solvent guest molecule inclusion. While a robust character capable of sensing guest molecules has been previously demonstrated in nanoporous framework materials displaying SCO (SCOFs),[16,17] this effect is highly novel for discrete complexes, in particular dinuclear materials.

Further to inducing the SCO properties of **1**·4 CH_2Cl_2 by thermal variation, it is possible to switch from the LS state to a metastable HS state by light irradiation (i.e., the LIESST effect). With irradiation at 10 K we see around 43% trapping of the metastable HS state, which relaxes again to the LS state with heating to about 75 K in the absence of irradiation. Thus, with an observed T(LIESST) value of 56 K and a $T_{1/2}$ value for the low temperature step of 88 K, by using the relationship $T(\mathrm{LIESST}) = T_0 - 0.3\,T_{1/2}$ we find a T_0 value of 82.4 K.[24,25] The four currently demonstrated T_0 values reported to date are: $T_0 = 100$ K (monodentate ligands),[27] 120 K (bidentate ligands),[27] 150 K (meridional ligands),[26] 200 K (three-dimensional network solids).[33] Here, the T_0 value for **1**·4 CH_2Cl_2 places it on the upper limit of materials with an effective Fe^{II} mononuclear ligand environment, rather than the $T_0 = 120$ K family observed for bidentate ligands. In **1**·4 CH_2Cl_2 we observe binding modes of the ddpp ligand to the Fe^{II} centers that result in relatively large chelation rings, thus allowing for significant flexibility around the metal centers.[7] Indeed, it is well known that vibrational aspects and hardness of the inner coordination sphere are key factors in enhancing the metastability of the light induced HS state, rather than the solid lattice effects largely associated with $T_{1/2}$ values. This finding also suggests that dinuclear materials may indeed follow the relationship $T(\mathrm{LIESST}) = T_0 - 0.3\,T_{1/2}$, which was compiled largely based on a database of mononuclear materials; however, further examples will need to be examined to confirm this.

Lastly, upon irradiation of the partially desolvated material **1**·CH_2Cl_2 with light, we observe essentially no LIESST activity. This is not so surprising when we look at its $T_{1/2}$ value of 200 K in combination with the assumed T_0 value of 100 K, which would result in a T(LIESST) value of about 40 K—a value that is unlikely to show much retention of a metastable HS state owing to competition between excitation and relaxation energies.[24] Notably, purely by guest manipulation, for example, between the full and partial solvated complexes, the photomagnetic properties of this system can be turned 'on' or 'off', thus producing a solvent sensing photomagnetic material reminiscent of the thermally addressable solvent sensing capabilities of porous SCO framework materials.[16,17]

Conclusions

In summary, we have shown that this family of dinuclear materials shows a diverse range of magnetic properties that can be manipulated through guest removal or exchange. The ability to tune SCO behavior in this series of materials is possible due to the robust nature of this system, which is provided by the array of intra- and intermolecular interactions, reminiscent of porous framework materials. Here, we have been able to selectively choose the presence of a one- or two-step spin transition by guest exchange—an important result towards tuning SCO properties. Additionally, this solvent tuning ability has allowed some key magneto-structural relationships to be gathered, in particular with regard to the presence of one- or two-step spin transitions, by direct structural comparisons within the one dinuclear system. We found, in general, that a two-step SCO is enabled when there are two distinct SCO centers per dinuclear unit, whereas a one-step SCO is found when there are crystallographically equivalent SCO centers in each dinuclear unit. Notably, the photomagnetic properties of this dinuclear material follow the same relationship (i.e., $T(\mathrm{LIESST}) = T_0 - 0.3\,T_{1/2}$)[24,25] as mononuclear complexes. Finally, we have shown that solvent variation in this dinuclear family can be exploited as a means to turn the photomagnetic properties 'on' or 'off'.

Experimental Section

General methods: All chemicals were obtained from Aldrich and Fluka and used without further purification.

Synthesis of 1·4 $CHCl_3$: A solution of iron(II) perchlorate hexahydrate (37.0 mg, 0.102 mmol) and ammonium thiocyanate (21.9 mg, 0.288 mmol) in ethanol (5 mL) was layered directly upon a solution of ddpp (41.2 mg, 0.0987 mmol) in chloroform (5 mL). Single crystals were formed within 24 h in close to quantitative yield.

Thermogravimetric analysis: Measurements were carried out on a TA instruments Hi-Res TGA 2950 Thermogravimetric Analyser. Decomposition analysis was performed over the temperature range of 25–500 °C at a heating rate of 1 °C min^{-1}. The atmosphere was controlled with a dry dinitrogen supply (0.1 L min^{-1}).

Crystallographic data collection and refinement: Single-crystal data were collected on a Bruker Smart 1000 CCD by using $Mo_{K\alpha}$ radiation ($\lambda = 0.71073$ Å) and equipped with an Oxford Instruments nitrogen gas cryostream. Single-crystal diffraction data for **1**·4 $CHCl_3$ were collected on the same crystal at 123(2) and 250(2) K. A separate crystal of **1**·4 $CHCl_3$ was mounted at 250 K and heated to 340 K at a rate of 20 K h^{-1} to form the trisolvated **1**·3 $CHCl_3$ (as per TGA measurements). The cryostream was then held at 340 K for 30 min before being cooled back down to 250 K at a rate of 360 K h^{-1}. Single-crystal diffraction data for **1**·3 $CHCl_3$ were collected at 250(2) and 110(2) K. A separate crystal of **1**·4 $CHCl_3$ was also mounted at 250 K and heated to 375 K at a rate of 15 K h^{-1} to form the monosolvated **1**·$CHCl_3$ (as per TGA measurements). The cryostream was held at 375 K for 30 min before being cooled back down to 250 K at a rate of 360 K h^{-1}. Single-crystal diffraction data for **1**·$CHCl_3$ were collected at 250(2) and 110(2) K. Empirical absorption corrections were applied to all data by using SADABS.[34] The structures were solved with SHELXS-86 and refined with SHELXL-97 from data reduced with SAINT+ V.6.45.[35] All non-hydrogen atoms in the structures were refined anisotropically and hydrogen atoms were generated by using the riding model.

CCDC-703883, CCDC-703884, CCDC-703885, CCDC-703886, CCDC-703887, and CCDC-703888 contain the crystal data for this paper. These data can be obtained free of charge from The Cambridge Crystallographic Data Centre via www.ccdc.cam.ac.uk/data_request/cif

Magnetic susceptibility measurements: Magnetic susceptibility data were collected by using a Quantum Design MPMS 5 SQUID magnetometer under an applied field of 1 T. Samples were placed in a quartz tube and great care was taken to avoid any solvent loss and/or torquing of crystallites of these potentially anisotropic [HS–HS] iron(II) species. Care was also taken to allow long thermal equilibration times at each temperature point. The sample of **1**·3 $CHCl_3$ was obtained by heating a sample of **1**·4 $CHCl_3$ at 67 °C for 3 h. The sample of **1**·$CHCl_3$ was obtained by heating a sample of **1**·4 $CHCl_3$ at 100 °C for 3 h. **1**·$CHCl_3$ samples were resolvated with either chloroform or dichloromethane through the addition of a few drops of neat solvent directly into the quartz tube. The fully desolvated material, **1**·Ø $CHCl_3$, was obtained through heating **1**·4 $CHCl_3$ at 200 °C for 3 h. Care was taken that the dinuclear unit did not dissolve and reform in this process. Additionally, the monosolvated material **1**·CH_2Cl_2 was prepared as reported previously[7] and was resolvated here with chloroform through immersion of the crystalline material in a small amount of solvent for 3 days. The degree of resolvation could not be determined accurately as the crystals were not suitable for X-ray crystallography after resolvation. We note that the parent chloroform-solvated material can also be generated through complete desolvation of the dichloromethane parent material, followed by immersion in neat solvent chloroform: this was confirmed by magnetic susceptibility measurements. Photomagnetic characterizations of **1**·4 CH_2Cl_2 and **1**·CH_2Cl_2 were performed by using a Kr^+ laser coupled through an optical fiber into the cavity of the MPMS-55 Quantum Design SQUID magnetometer operating at 2 T. Samples were prepared as a thin layer (ca. 0.1 mg) to promote maximal penetration of the irradiating light. Solvent loss was minimized by rapid sample mounting and minimal purging of the SQUID airlock. The sample weight was obtained by comparing its thermal SCO behavior with that of a larger, accurately weighed sample.[24] The sample was first slowly cooled to 10 K to ensure that trapping of HS species at low temperatures did not occur. Irradiation to photosaturation was carried out a number of times by using different wavelengths (i.e., 337/356.4 nm; 406.7/415.4 nm; 530.2 nm; 647.1/676.4 nm, and 752.5/799.3 nm) to determine the most efficient source, and with power intensity up to 5 mW cm^{-2}. The sample in the LS state was then irradiated with green light ($\lambda = 530.2$ nm at 5 mW cm^{-2}), the most efficient, until photosaturation was reached. Then, in the absence of irradiation, the temperature was increased in 1 K steps to 100 K to determine the T(LIESST) value, and then changed in 3 K steps over the range 100–290–10 K to follow the thermal SCO. The extreme of the $d\chi_M T/dT$ versus T plot gave the T(LIESST) values, which is defined as the temperature at which the light-induced HS information is erased.[24] At 10 K, the sample was again irradiated to photosaturation and, in the absence of irradiation, the relaxation kinetics at 10, 50, 55, 58 and 60 K were measured.

Optical reflectivity measurements: Reflectivity was investigated by using a home-built set-up coupled with a SM240 spectrometer (Opton Laser International), which allows both the reflectivity spectra to be collected in the range of $\lambda = 450$–950 nm at a given temperature and the temperature dependence of the signal at a selected wavelength (±2.5 nm) between 5 and 290 K to be followed. Samples were irradiated with light over the entire temperature range. The diffuse reflected signal was calibrated by using activated charcoal (Merck) as a black standard and barium sulfate ($BaSO_4$, DIN50533, Merck) as a white standard. The instrument is also equipped with an optical detector, which collects the entire reflected intensity and gives the total reflectivity signal as a function of temperature. The source of the white light consists of a halogen lamp emitting between 350–2400 nm. This analysis was performed directly on a thin layer of a polycrystalline sample with a small amount of liquid solvent added to avoid desolvation, but without any dispersion in a matrix.

Acknowledgements

The Australian Research Council, ARC, is thanked for providing a Discovery Grant to support this work. Financial support for the photomagnetic LIESST work was kindly provided by a French–Australia FAST/DEST grant and this allowed the Australian participants to travel to Bordeaux to carry out measurements. The authors would also like to thank the Aquitaine Region for supporting the development of the international platform of photomagnetism.

[1] a) O. Kahn, *Molecular Magnetism*, VCH, Weinheim, **1993**; b) P. Gütlich, A. Hauser, *Coord. Chem. Rev.* **1990**, *97*, 1–22; c) P. Gütlich, A. Hauser, H. Spiering, *Angew. Chem.* **1994**, *106*, 2109–2141; *Angew. Chem. Int. Ed. Engl.* **1994**, *33*, 2024–2054; d) A. Hauser, *Coord. Chem. Rev.* **1991**, *111*, 275–290.

[2] P. Gütlich, H. A. Goodwin, *Top. Curr. Chem.* **2004**, *233*, 1–47.

[3] O. Kahn, C. J. Martinez, *Science* **1998**, *279*, 44–48.

[4] J.-F. Létard, P. Guionneau, L. Goux-Capes, *Top. Curr. Chem.* **2004**, *235*, 221–249.

[5] K. S. Murray, C. J. Kepert, *Top. Curr. Chem.* **2004**, *233*, 195–228.

[6] a) J. A. Real, A. B. Gaspar, V. Niel, M. C. Muñoz, *Coord. Chem. Rev.* **2003**, *236*, 121–141; b) E. Trzop, M. Buron-Le Cointe, H. Cailleau, L. Toupet, G. Molnár, A. Bousseksou, A. B. Gaspar, J. A. Real, E. Collet, *J. Appl. Crystallogr.* **2007**, *40*, 158–164.

[7] J. J. Amoore, C. J. Kepert, J. D. Cashion, B. Moubaraki, S. M. Neville, K. S. Murray, *Chem. Eur. J.* **2006**, *12*, 8220–8227.

[8] M. H. Klingele, B. Moubaraki, J. D. Cashion, K. S. Murray, S. Brooker, *Chem. Commun.* **2005**, 987–989.

[9] K. S. Murray, *Eur. J. Inorg. Chem.* **2008**, 3101–3121.

[10] a) K. Nakano, S. Kawata, K. Yoneda, A. Fuyuhiro, T. Yagi, S. Nasu, S. Morimoto, S. Kaizaki, *Chem. Commun.* **2004**, 2892–2893; b) B. A. Leita, B. Moubaraki, K. S. Murray, J. P. Smith, J. D. Cashion, *Chem. Commun.* **2004**, 156–157.

[11] J. A. Real, H. Bolvin, A. Bousseksou, A. Dworkin, O. Kahn, F. Varret, J. Zarembowitch, *J. Am. Chem. Soc.* **1992**, *114*, 4650–4658.

[12] a) C. M. Grunert, S. Reiman, H. Spiering, J. A. Kitchen, S. Brooker, P. Gütlich, *Angew. Chem.* **2008**, *120*, 3039–3041; *Angew. Chem. Int. Ed.* **2008**, *47*, 2997–2999; b) J. A. Kitchen, S. Brooker, *Coord. Chem. Rev.* **2008**, *252*, 2072–2092; c) B. Weber, E. S. Kaps, J. Obel, K. Achterhold, F. G. Parak, *Inorg. Chem.* **2008**, *47*, 10779–10787.

[13] V. Ksenofontov, A. B. Gaspar, V. Niel, S. Reiman, J. A. Real, P. Gütlich, *Chem. Eur. J.* **2004**, *10*, 1291–1298.

[14] S. Brooker, P. G. Plieger, B. Moubaraki, K. S. Murray, *Angew. Chem.* **1999**, *111*, 424–426; *Angew. Chem. Int. Ed.* **1999**, *38*, 408–410.

[15] A. B. Gaspar, M. C. Muñoz, J. A. Real, *J. Mater. Chem.* **2006**, *16*, 2522–2533.

[16] G. J. Halder, C. J. Kepert, B. Moubaraki, K. S. Murray, J. D. Cashion, *Science* **2002**, *298*, 1762–1765.
[17] a) S. M. Neville, B. Moubaraki, K. S. Murray, C. J. Kepert, *Angew. Chem.* **2007**, *119*, 2105–2108; *Angew. Chem. Int. Ed.* **2007**, *46*, 2059–2062; b) S. M. Neville, G. J. Halder, K. W. Chapman, M. D. Duriska, P. D. Southon, J. D. Cashion, J.-F. Létard, B. Moubaraki, K. S. Murray, C. J. Kepert, *J. Am. Chem. Soc.* **2008**, *130*, 2869–2876; c) G. J. Halder, K. W. Chapman, S. M. Neville, B. Moubaraki, K. S. Murray, J.-F. Létard, C. J. Kepert, *J. Am. Chem. Soc.* **2008**, *130*, 17552–17562; d) M. Ohba, K. Yoneda, G. Agustí, M. C. Muñoz, A. B. Gaspar, J. A. Real, M. Yamasaki, H. Ando, Y. Nakao, S. Sakaki, S. Kitagawa, *Angew. Chem.* **2009**, *121*, 4861–4865; *Angew. Chem. Int. Ed.* **2009**, *48*, 4767–4771; e) P. D. Southon, L. Liu, E. A. Fellows, D. J. Price, G. J. Halder, K. W. Chapman, B. Moubaraki, K. S. Murray, J.-F. Létard, C. J. Kepert, *J. Am. Chem. Soc.* **2009**, *131*, 10998–11009; S. M. Neville, G. J. Halder, K. W. Chapman, M. B. Duriska, B. Moubaraki, K. S. Murray, C. J. Kepert, *J. Am. Chem. Soc.* **2009**, *131*, 12106–12108.
[18] a) G. Chastanet, A. B. Gaspar, J. A. Real, J.-F. Létard, *Chem. Commun.* **2001**, 819–820; b) C. M. Grunert, J. Schweifer, P. Weinberger, W. Linert, K. Mereiter, G. Hilscher, M. Muller, G. Wiesinger, P. J. van Koningsbruggen, *Inorg. Chem.* **2004**, *43*, 155–165; c) R. Kitashima, S. Imatomi, M. N. Yamada, Y. Maeda, *Chem. Lett.* **2005**, *34*, 1388–1389; d) N. Ortega-Villar, A. L. Thompson, M. C. Muñoz, V. M. Ugalde-Saldívar, A. E. Goeta, R. Moreno-Esparza, J. A. Real, *Chem. Eur. J.* **2005**, *11*, 5721–5734.
[19] a) See a series of articles on "Molecular Spintronics and Quantum Computing" in *J. Mater. Chem.* **2009**, *19*, 670–1760, with Editorial by E. Coronado, A. J. Epstein, *J. Mater. Chem.* **2009**, *19*, 1670–1671; b) M. Affronte, *J. Mater. Chem.* **2009**, *19*, 1731–1737; c) F. Troiani, A. Ghirri, M. Affronte, S. Carretta, P. Santini, G. Amoretti, S. Piligkos, G. Timco, R. E. P. Winpenny, *Phys. Rev. Lett.* **2005**, *94*, 207208; d) L. N. Dawe, K. V. Shuvaev, L. K. Thompson, *Inorg. Chem.* **2009**, *48*, 3323–3341.
[20] I. Yildiz, E. Deniz, F. M. Raymo, *Chem. Soc. Rev.* **2009**, *38*, 1859–1867.
[21] G. Chastanet, C. Carbonera, C. Mingotaud, J.-F. Létard, *J. Mater. Chem.* **2004**, *14*, 3516–3523.
[22] F. M. Raymo, *Adv. Mater.* **2002**, *14*, 401–414.
[23] N. Ould Moussa, E. Trzop, S. Mouri, S. Zein, G. Molnár, A. B. Gaspar, E. Collet, M. Buron-Le Cointe, J. A. Real, S. Borshch, K. Tanaka, H. Cailleau, A. Bousseksou, *Phys. Rev. B* **2007**, *75*, 054101.
[24] J.-F. Létard, *J. Mater. Chem.* **2006**, *16*, 2550–2559.
[25] J.-F. Létard, P. Guionneau, O. Nguyen, J. S. Costa, S. Marcén, G. Chastanet, M. Marchivie, L. Goux-Capes, *Chem. Eur. J.* **2005**, *11*, 4582–4589.
[26] C. Carbonera, J. S. Costa, V. A. Money, J. Elhaïk, J. A. Howard, M. A. Halcrow, J.-F. Létard, *Dalton Trans.* **2006**, 3058–3066.
[27] J.-F. Létard, L. Capes, G. Chastanet, N. Moliner, S. Létard, J. A. Real, O. Kahn, *Chem. Phys. Lett.* **1999**, *313*, 115–120.
[28] a) S. Marcén, L. Lecren, L. Capes, H. A. Goodwin, J.-F. Létard, *Chem. Phys. Lett.* **2002**, *358*, 87–95; b) V. A. Money, J. S. Costa, S. Marcén, G. Chastanet, J. Elhaïk, M. A. Halcrow, J. A. Howard, J.-F. Létard, *Chem. Phys. Lett.* **2004**, *391*, 273–277.
[29] a) J.-F. Létard, J. A. Real, N. Moliner, A. B. Gaspar, L. Capes, O. Cador, O. Kahn, *J. Am. Chem. Soc.* **1999**, *121*, 10630–10631; b) J.-F. Létard, C. Carbonera, J. A. Real, S. Kawata, S. Kaizaki, *Chem. Eur. J.* **2008**, *14*, 4146–4155.
[30] P. Guionneau, M. Marchivie, G. Bravic, J.-F. Létard, D. C. Chasseau, *Top. Curr. Chem.* **2004**, *234*, 97–128.
[31] J.-F. Létard, P. Guionneau, L. Rabardel, J. A. K. Howard, A. E. Goeta, D. Chasseau, O. Kahn, *Inorg. Chem.* **1999**, *38*, 4432–4441.
[32] V. Niel, A. L. Thompson, M. C. Muñoz, A. Galet, A. E. Goeta, J. A. Real, *Angew. Chem. Int. Ed.* **2003**, *115*, 3890–3893; *Angew. Chem. Int. Ed.* **2003**, *42*, 3760–3763.
[33] N. Shimamoto, S.-S. Ohkoshi, O. Sato, K. Hashimoto, *Inorg. Chem.* **2002**, *41*, 678–684.
[34] SADABS, empirical adsorption correction program for area detector data, G. M. Sheldrick, University of Göttingen, Göttingen, **1996**.
[35] a) SMART, SAINT and XPREP; area detector and data integration and reduction software, Bruker Analytical Instruments Inc., Madison, Wisconsin, USA, **1995**; b) SHELXTL, program for crystal structure solution and refinement, Bruker Analytical X-ray Instruments Inc., Madison, Wisconsin (USA), **1997**; c) SHELXL-97, program for crystal structural solution and refinement, Bruker Analytical Instruments Inc., Madison, **1997**.

Received: July 1, 2009
Revised: September 3, 2009
Published online: December 22, 2009

